Warping for Trim Statics

Dongliang Zhang[*1], *Xin Wang*[1], *Yunsong Huang*[1], *Gerard Schuster*[1], *1. King Abdullah University of Science and Technology (KAUST)*

SUMMARY

The quality of migration images depends on the accuracy of the velocity model. For large velocity errors, the migration image is strongly distorted, which unflattens events in the common image gathers and consequently leads to a blurring in the stacked migration image. To mitigate this problem, we propose dynamic image warping to flatten the common image gathers before stacking and to enhance the signal-to-noise ratio of the migration image. Numerical tests on the Marmousi model and GOM data show that image warping of the prestack images followed by stacking leads to much better resolved reflectors than the original migration image. The problem, however, is that the reflector locations have increased uncertainty because the wrong velocity model is still used.

INTRODUCTION

Migration velocity analysis is crucial for any migration method, where the quality of the migration image decreases if the velocity errors increase. In order to get a migration velocity model close to the true one, traveltime inversion (Langan et al., 1984; Bishop et al., 1985; Luo and Schuster, 1991) inverts the traveltimes for the background velocity so that the calculated travel time matches the observed travel time. However, traveltime inversion can only estimate the low wavenumber portion of velocity model and the depth of inversion is limited. In contrast, migration velocity analysis (Symes and Kern, 1994) uses moveout residual in the common image gathers to update the velocity, which is both robust and practical. Another method is full waveform inversion (Tarantola, 1984; Bunks et al., 1995; Pratt, 1999; Pratt and Shipp, 1999) developed to obtain more accurate velocities by inverting both phase and amplitude. However, no matter what method is applied, the migration velocity model always contains errors.

Hale (2013) proposed the dynamic image warping (DIW) method to calculate the time shifts of two sets of related seismic traces. After accumulating and backtracking alignment errors, DIW can produce reasonable estimates of the time shifts which vary with the time and space. Using these time shifts, one of the seismic data sets can be approximately aligned with the other sets.

In our paper, we simply use DIW to flatten the CIGs before stacking. The vertical space shifts between each trace of the CIGs and the standard traces are calculated by DIW. Using these vertical space shifts, common image gathers are flattened. After stacking these flattened CIGs, the signal-to-noise ratio of the migration image is enhanced.

In this paper, we apply warping stacking to synthetics computed for the Marmousi model and the GOM data to demonstrate the effectiveness of this method. In the numerical tests, the common image gathers are indexed by the shot number. In general, warping and stacking for trim statics can be applied to any other type of common image gather.

DYNAMIC IMAGE WARPING OF CIGS

Due to the errors in the velocity model, common image gathers often have unflattened events, and stacking these gathers will produce a blurred migration image. Now we use the dynamic image warping to flatten the CIGs before stacking. Hale (2013) proposed the DIW to calculate the time shifts between two sets of related recorded seismic data. We extend DIW to find the space shifts l between two traces in the common image gather. Let $m(z;x,s)$ denote one trace of a common image gather, where z is depth, x is the horizontal location of the common image gathers, and s is the shot number. The function $m_c(z;x)$ is the standard trace defined by

$$m_c = \frac{1}{s_n - s_1}\int m(z;x,s)ds, \tag{1}$$

where, s_1, s_n are the beginning and ending shot numbers. Finding a shift distribution $l(z;x,s)$ is to solve the following constrained optimization problem:

$$u = \underset{l}{argmin} D(l), \tag{2}$$

subject to

$$|\frac{\partial u}{\partial z}| \leq \sigma_z, |\frac{\partial u}{\partial x}| \leq \sigma_x, |\frac{\partial u}{\partial s}| \leq \sigma_s, \tag{3}$$

where $\sigma_z, \sigma_x, \sigma_s$ are specified constraint values. $D(l)$ measures the L2 distance between all the traces and the standard trace in the common image gathers, and is defined by

$$D(l) = \frac{1}{2}\int (m(z+l(z;x,s);x,s) - m_c(z;x))^2 dzdxds. \tag{4}$$

The dynamic warping method can find the minimizing path u that minimizes the distance D. Constraints for equation 3 control the rates at which shifts vary in directions z,x,s. These constraints ensure that the space shifts neither decrease nor increase too rapidly.

Figure 1 shows an example of the dynamic warping applied to estimate shifts between two traces, $f(z)$ (Figure 1a) and its warped version $g(z)$ (1b). For this example, the known shifts between $f(z)$ and $g(z)$ correspond to a sine function, which are indicated by the dotted line in Figure 1c. Dynamic warping correctly estimates the shifts (solid line), meanwhile, cross-correlation fails (dashed line), especially when the shifts change rapidly.

DOI http://dx.doi.org/10.1190/segam2014-0281.1

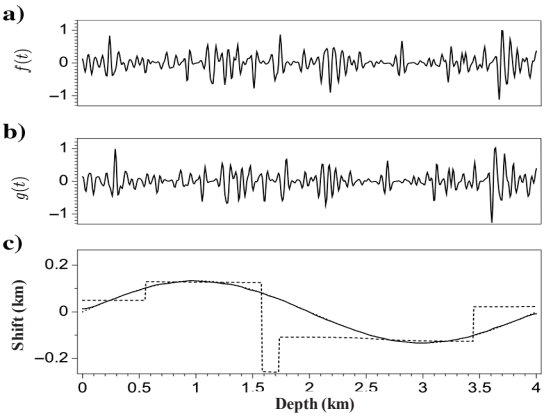

Figure 1: a). A trace from a common image gather $f(z)$. b). Its warped version is $g(z)$. c). The shifts follow a sine function indicated by the dotted line. The solid line represents the estimated shifts by dynamic warping and the dash line is the result of cross-correlation. Figures courtesy of Ma and Hale (2013).

NUMERICAL EXAMPLES

In this section, we will apply warping and stacking to synthetics generated for the Marmousi model and GOM data.

MARMOUSI MODEL

Warping stacking is applied to the migrated images obtained from the Marmousi data shown in Figure 2a. The model size is 351×950 gridpoints with a gridpoint spacing of 10 m. There are 475 shots/receivers distributed on the surface with 20 m interval. Figure 2b shows the migration velocity with a error, and the corresponding RTM image is shown in Figure 3a. In the deep part of the migration image, the events are discontinuous and distorted, so it is difficult to determine the location of the structure.

In order to mitigate the impact of velocity errors on the migration image, we apply dynamic image warping to the common image gather indexed by the shot number shown in Figure 4a. There are 101 traces in the common image gather, and the location of the shot for the middle trace is same as the location of the common image gathers. To avoid the large warp values that might distort the DIW result, the shallow parts are muted, as shown in Figure 4a. The target of seismic exploration is usually in the deep subsurface, the velocity in the shallow area is usually more accurate than the deep area, so muting the shallow image for DIW is reasonable. Compared to Figure 4a, the common image gather becomes flatter after using dynamic warping in Figure 4b. Figure 4c shows the vertical space shifts in the common image gather. Figure 5a shows another common image gather located at 4.5 km, and Figure 5b shows the common image gather after using dynamic image warping. At this location, large velocity errors promote disorder in the common image gather. Even in this situation, dynamic image warping partly flattens the events in the common image gathers. The corresponding vertical space shifts are shown in figure 5c.

Stacking the common image gathers after warping produces the RTM image shown in Figure 3b. Compared to Figure 3a, the image using warping stacking has a high signal-to-noise ratio and structures in the deep part are more clearly delineated. Figures 6a-6b show the zoomed views of the RTM image before and after warping stacking in the middle part. The RTM image after warping and stacking is more continuous, and includes fewer artifacts and higher wavenumbers. Stacking the unaligned event in the common image gathers cancels the high wavenumbers. If the common image gathers are flat, the high wavenumbers can be preserved after stacking. The zoomed views of RTM image before and after warping and stacking in the deep portion are shown in the Figures 6c-6d. Comparing these two results, the structure in the image using warping and stacking is more clearly delineated than in Figure 6c.

GOM DATA

Dynamic image warping is applied to the common image gathers computed by plane-wave migration for GOM data. Each common image gather shown in Figure 7a were computed from 31 planewaves with ray parameters (p) from -0.333 ms/m to 0.333 ms/m. After dynamic image warping, the flatter common image gathers are shown in Figure 7b, and the corresponding vertical space shifts are shown in 7c. After stacking these warped common image gathers, the final migration image is shown in Figure 8b. Compared to the original migration image shown in Figure 8a, the migration image after warping and stacking contains a higher signal-noise ratio. The zoom views of two different areas are shown in Figure 9. Both comparisons suggest the events in the stacked migration image after warping and stacking are more continuous.

CONCLUSIONS

We present the trim statics by warping and stacking CIGs. The key is to flatten the common image gathers by warping, then stack them to form the final migration image. The main benefits are that signal-noise ratio is enhanced in the migration image and some structures are more clearly delineated, and the high wavenumbers of the migration image are preserved.

Numerical tests on Marmousi data and GOM data demonstrate the effectiveness of the warping and stacking CIGs. In both the middle and deep portions, the RTM image of Marmousi model with warping stacking shows fewer artifacts, better continuity and more illuminated reflectors.

ACKNOWLEDGMENTS

We thank the KAUST Supercomputing Lab for the computer cycles they donated to this project. We are especially grate-

DOI http://dx.doi.org/10.1190/segam2014-0281.1

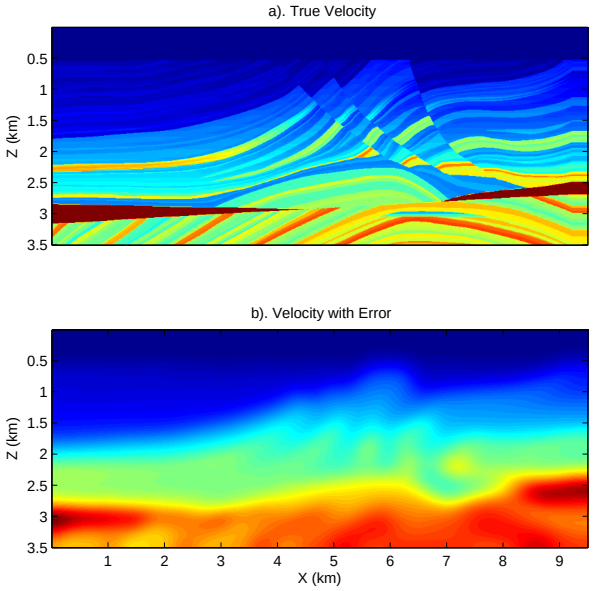

Figure 2: a). True velocity of Marmousi model. b). Migration velocity model with error.

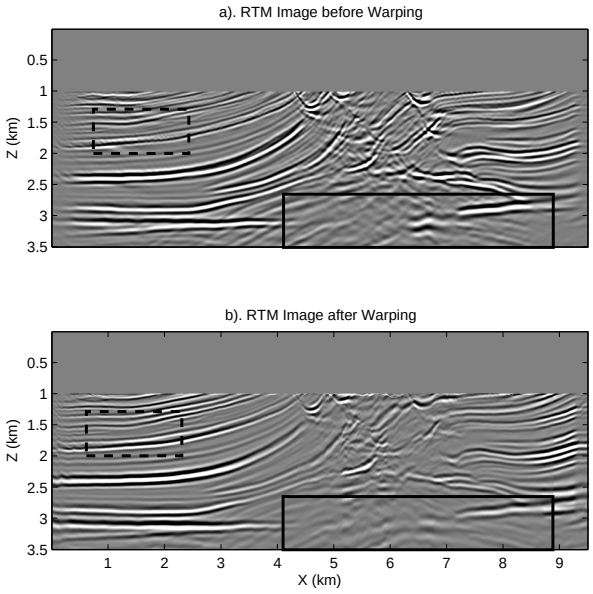

Figure 3: a). RTM image using migration velocity shown in Figure 2b, the shallow part is muted to compare the result after using warping and stacking. b). RTM image after using warping and stacking.

ful for the use of the SHAHEEN supercomputer. We also acknowledge the support of the CSIM sponsors (http://csim.kaust.edu.s

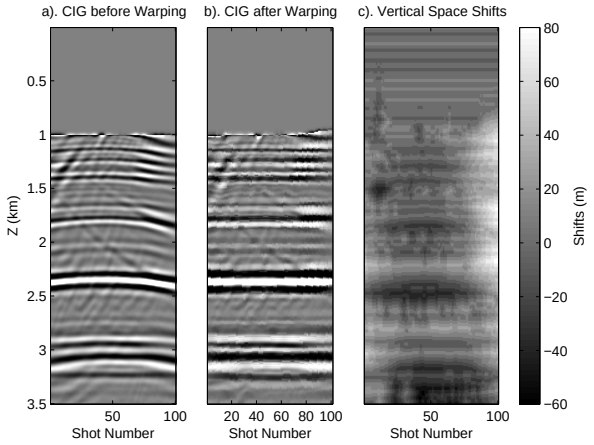

Figure 4: a). Common image gather at 2 km. b) The common image gathers after using dynamic image warping. c). Vertical space shifts.

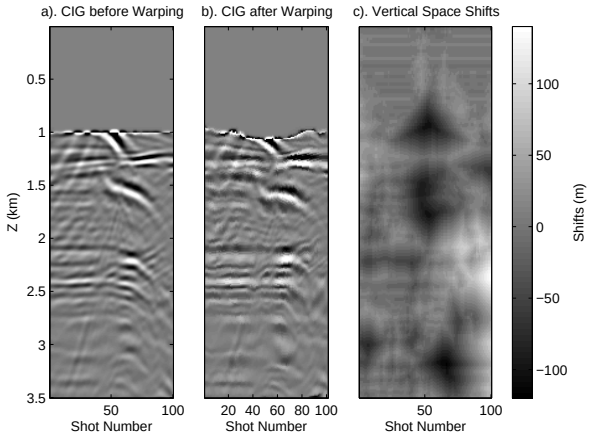

Figure 5: a). Common image gathers at 4.5 km with the shallow image mutted. b) The common image gathers after using dynamic image warping. c). Vertical space shifts.

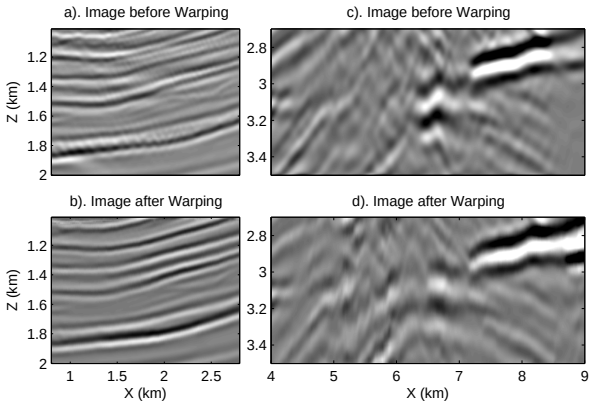

Figure 6: Zoom views of a) RTM images before and b) after using warping and stacking in middle part (boxes of dashed lines shown in Figure 3), and c), d) in the deep part (boxes of solid lines shown in Figure 3).

DOI http://dx.doi.org/10.1190/segam2014-0281.1

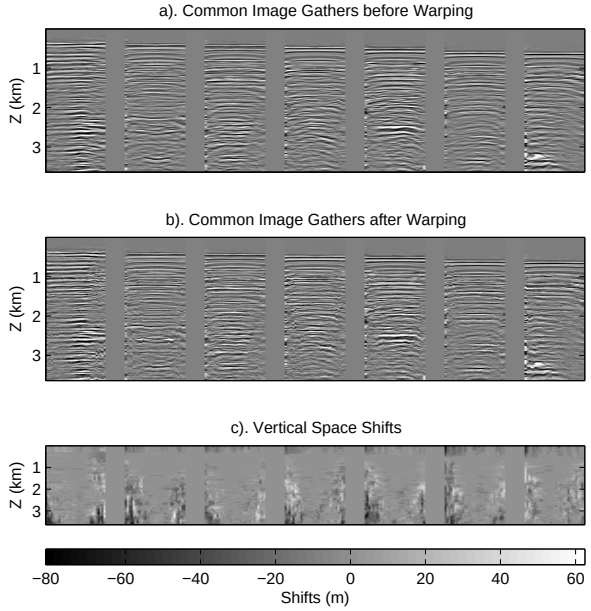

Figure 7: Common image gathers a) before and b) after using dynamic image warping. c). Vertical space shifts.

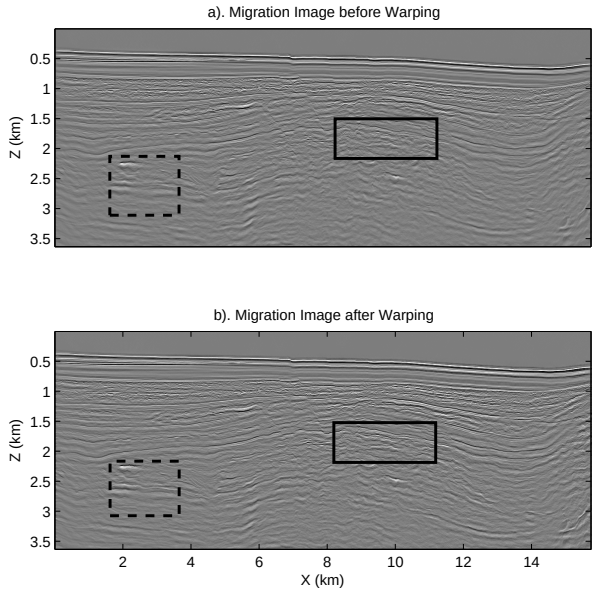

Figure 8: Migration images a) before and b) after using warping and stacking.

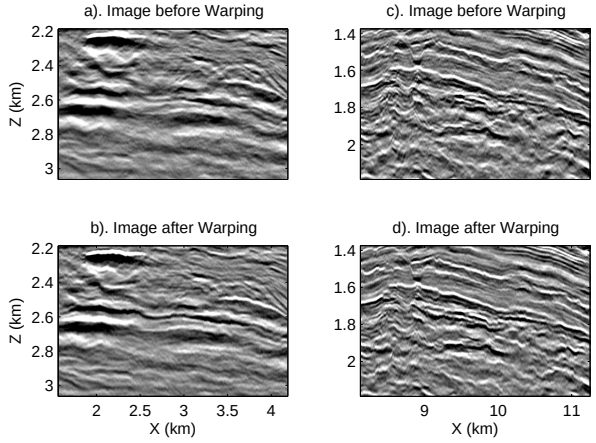

Figure 9: Zoom views of migration images a) before and b) after using warping and stacking in the area of box the dashed lines shown in Figure 8), and c), d) in the area of box solid lines shown in Figure 8.

DOI http://dx.doi.org/10.1190/segam2014-0281.1

http://dx.doi.org/10.1190/segam2014-0281.1

EDITED REFERENCES

Note: This reference list is a copy-edited version of the reference list submitted by the author. Reference lists for the 2014 SEG Technical Program Expanded Abstracts have been copy edited so that references provided with the online metadata for each paper will achieve a high degree of linking to cited sources that appear on the Web.

REFERENCES

Bishop, T., K. Bube, R. Cutler, R. Langan, P. Love, J. Resnick, R. Shuey, D. Spindler, and H. Wyld, 1985, Tomographic determination of velocity and depth in laterally varying media : Geophysics, **50**, 903–923, http://dx.doi.org/10.1190/1.1441970.

Bunks, C., F. Saleck, S. Zaleski, and G. Chavent, 1995, Multiscale seismic waveform inversion: Geophysics, **60**, 1457–1473, http://dx.doi.org/10.1190/1.1443880.

Hale, D., 2013, Dynamic warping of seismic images: Geophysics, **78**, no. 2, S105–S115, http://dx.doi.org/10.1190/geo2012-0327.1.

Langan, R., I. Lerche, R. Cutler, T. Bishop, and N. J. Spera, 1984, Seismic tomography: The accurate and efficient tracing of rays through heterogeneous media : 54th Annual International Meeting, SEG, Expanded Abstracts, 713–715, http://dx.doi.org/10.1190/1.1894309 .

Luo, Y., and G. Schuster, 1991, Wave-equation traveltime inversion: Geophysics, **56**, 645–653, http://dx.doi.org/10.1190/1.1443081.

Ma, Y., and D. Hale, 2013, Wave-equation reflection traveltime inversion with dynamic warping and full-waveform inversion: Geophysics, **78**, no. 6, R223–R233, http://dx.doi.org/10.1190/geo2013-0004.1.

Pratt, R., 1999, Seismic waveform inversion in the frequency domain, Part 1: Theory and verification in a physical scale model: Geophysics, **64**, 888–901, http://dx.doi.org/10.1190/1.1444597.

Pratt, R., and R. Shipp, 1999, Seismic waveform inversion in the frequency domain, Part 2: Fault delineation in sediments using crosshole data: Geophysics, **64**, 902–914, http://dx.doi.org/10.1190/1.1444598.

Symes, W. W., and M. Kern, 1994, Inversion of reflection seismograms by differential semblance analysis: Algorithm structure and synthetic examples: Geophysical Prospecting, **42**, 565–614, http://dx.doi.org/10.1111/j.1365-2478.1994.tb00231.x.

Tarantola, A., 1984, Inversion of seismic reflection data in the acoustic approximation: Geophysics, **49**, 1259–1266, http://dx.doi.org/10.1190/1.1441754.